JACS
JOURNAL OF THE AMERICAN CHEMICAL SOCIETY
Article
pubs.acs.org/JACS

Unexpected Chirality of Nanoparticle Dimers and Ultrasensitive Chiroplasmonic Bioanalysis

Xiaoling Wu,[†,#] Liguang Xu,[†,#] Liqiang Liu,[†] Wei Ma,[†] Honghong Yin,[†] Hua Kuang,*[,†] Libing Wang,[†] Chuanlai Xu,[†] and Nicholas A. Kotov*[,‡]

[†]State Key Lab of Food Science and Technology, School of Food Science and Technology, Jiangnan University, Wuxi, JiangSu 214122, P.R. China

[‡]Departments of Chemical Engineering, Materials Science, and Biomedical Engineering, and Biointerfaces Institute, University of Michigan, Ann Arbor, Michigan 48109, United States

Supporting Information

ABSTRACT: Chiral assemblies of nanoparticles (NPs) are typically constructed with helical or tetrahedral geometries. Simple pairs of NPs are not expected to display chirality due to basic symmetry considerations made under the assumption of their spherical geometry. In this study we demonstrate that assemblies consisting of two metallic NPs do possess chirality and strongly rotate polarization of light. Their chiroplasmonic properties are attributed to the prolate geometry of individual colloidal particles. When bridged by biomolecules, the NP pairs acquire scissor-like geometry, with the long axes of NPs forming an angle of ~9°. This small dihedral angle results in chirality of the NP pair, while the consistency of its sign due to the specific conformation of the bridging biomacromolecules breaks the enantiomeric equivalence of the NP pairs. Strong polarization rotation in these nanoassemblies makes possible their utilization in biological analysis. Heterodimers of gold and silver NPs were made using antibody−antigen bridges. Taking advantage of their chiroplasmonic properties, we investigated their bioanalitical potential for detection of an environmental toxin, microcystin-LR, and a cancer biomarker, prostate-specific antigen. The order-of-magnitude improvements in limits of detection compared to all other analytical techniques are attributed to plasmonic enhancement of intrinsic chirality of biological compounds, strong optical coupling of photons with NP assemblies with twisted geometries, and signal amplification due to the bisignate nature of circular dichroism bands.

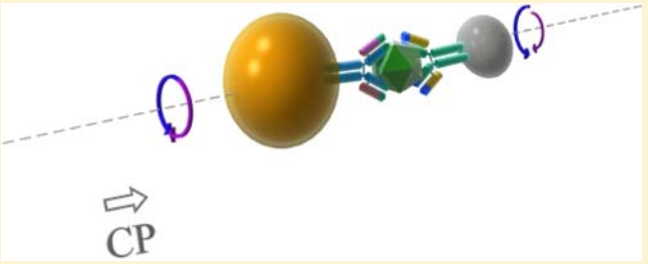

INTRODUCTION

Biosensing is central for medical, chemical, environmental, and other fields of science.[1−3] Plasmonic nanoparticles (NPs) make possible new biosensing techniques based primarily on the red-to-blue spectral shift of the absorption bands upon formation of closely spaced plasmonic superstructures.[4−6] Other optical effects related to coupling of polaron oscillations in adjacent NPs, exemplified by surface-enhanced Raman spectroscopy (SERS),[7−9] and other analytical techniques,[6,10−15] exemplified by bio-bar-code assay,[14,15] also show remarkable sensitivity and versatility. Despite exceptional progress in single-molecule analytical capabilities observed for selected small analytes,[16,17] there is still a great need to improve the detection limits for a large variety of biological compounds, especially in complex biological media[1,18,19] and analytes with larger molecular mass. Note that some NP-based techniques are applicable to small peptides,[20] while larger proteins are more difficult to detect using plasmonic coupling methods due to the fast decay of electrical field intensity with the distance between the plasmonic centers.[11,21] A chiroplasmonic method based on twisted assemblies of gold nanorods[22] demonstrated exceptional sensitivity to long strands of DNA due to the strong polarization rotation of light.[23] Polarization rotation was found to be less dependent on the gap between the gold nanorods than on the intensity of the hot spot essential for SERS or plasmonic colorimetry. This unusual feature of the chiroplasmonic method makes it possible to put forward a much-needed way to detect biological compounds with a wide range of diameters while simultaneously improving limits of detection (LODs)[18] and discovering fundamentally novel optical effects for the nanoscale assemblies.

We hypothesized that plasmonic effects observed in chiral assemblies of NPs can also be used for analytical purposes. Chiral NP assemblies represent one of the most dynamic areas of current research.[24−41] However, they been viewed primarily as tools for construction of chiral meta-materials.[42,43] Early studies of their use in stereoselective catalysis[44,45] and enantioselective separation of chiral nanostructures[41] should also be noted. Although chiroplasmonic biosensing is still in the very early stages of its development,[21,23] attomolar LODs for long strands of DNA have been recently demonstrated.[23] This is a milestone in its own sense for DNA detection, but we believe this is not the limit, and the bioanalytical applications of

Received: September 15, 2013
Published: November 18, 2013

   dx.doi.org/10.1021/ja4095445 | J. Am. Chem. Soc. 2013, 135, 18629−18636

the chiroplasmonic properties can be expanded. The use of chiral NP constructs in solution, regardless of their geometry, would be advantageous due to the simplicity of their preparation, the diversity of their compositions, and the wide spectrum of potential chiroplasmonic bands found in their assemblies.[46,27]

With this premise in mind, we decided to investigate NP assemblies made from two different metallic components: AgNPs and AuNPs. To our great surprise, we learned that even the simplest forms of heteroparticle assemblies—dimers made from one AgNP and one AuNP connected by antigen−antibody bridges, also known as heterodimers—display startlingly intense circular dichroism (CD) bands. The chirality of such structures is unexpected because a pair of spherical objects, e.g. NPs, can be perfectly superimposed with its mirror image. Our study revealed that the chirality of NP pairs originates from nonideality of their shape. Individual particles are not spherical but prolate, while their dimers have scissor-like geometry with two long NP axes forming a consistent dihedral angle. Similar effects were recently observed in twisted nanorod pairs,[22] although for them the possibility of misalignment of the long axes, leading to the formation of twisted chiral systems, was less of a surprise.[47] We also found that the heterodimers can be used as versatile biosensing platforms, taking advantage of bisignate CD bands. Moreover, the LODs found for two biomacromolecules—namely a relatively small, persistent peptide, microcystin-LR (MCLR), representative of persistent environmental pollutants, and prostate-specific antigen (PSA), representative of cancer biomarkers—were 8×10^{-13} and 1.5×10^{-20} M for MCLR and PSA, respectively. These LODs are markedly better than those of any other techniques reported so far for these essential biological analytes.

RESULTS AND DISCUSSION

Construction of the Heterodimers. Chiral heterodimers were assembled from AuNPs functionalized with antibodies using protocols described in the Experimental Section.[5] Corresponding antibodies (mAbs) were conjugated to AuNPs in a 1:1 molar ratio (see Experimental Section).[48] Following the same synthetic protocol, we also prepared AgNPs that carried biomacromolecules similar to the target analyte, i.e., MCLR or PSA, but with lower affinity to mAb. These biomacromolecules will be denoted as competitive antigens (CAgs). The functionalized AgNPs and AuNPs were assembled into dimers following the standard antigen−antibody immunoreaction (Figure 1).[39]

Chiroptical Properties of Heterodimers. To study the chiroplasmonic properties of NP assemblies, AuNPs were modified with anti-MCLR mAbs. At the same time, AgNPs were modified with BSA-MCLR construct; in this case this biomacromolecular conjugate served as a CAg to pair with MCLR as the target analyte. When mixed, these two types of NPs form heterodimers bridged by the mAb-CAg intermolecular complex. Their formation was identified by transmission electron microscopy (TEM, Figures 2E−G and 3G, H) and dynamic light scattering (DLS, Figure S1). It was also confirmed by the shifts of the silver and gold UV−vis plasmon bands to the red and to the blue sides of the spectrum, respectively (Figures 2A and S2).

The majority of the dimers are formed in the first 40 min (Figures 2A,B and S3), which matches the typical timing of antigen−antibody immunoreactions.[39] The dimers were formed in high yield of 84.1%, with minimal amount of NPs

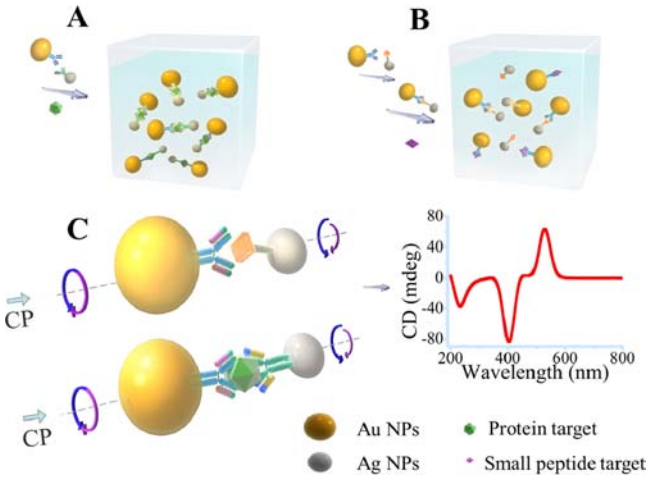

Figure 1. Schematic illustration for the assembly of NP hetero dimers and their use for biological analysis. (A,B) The NP dimer was assembled from AuNPs and AgNPs, which were functionalized with complementary biomacromolecules (A). For the detection of small peptides, exemplified by MCLR, the competitive immunorecognition assay was chosen to demonstrate its applicability to biological analysis. It results in a decrease of the CD amplitude (B). For detection of the fairly large proteins, exemplified by PSA, we used sandwich immunoassay mode. (C) Schematics of the NP dimers bridged by immunocomplexes used in competitive and sandwich immunoassays.

remaining as freely suspended colloid. There was less than 3% of multimers (trimers, tetramers, etc.) formed from nonspecific adsorption. Synchronously with the formation of NP dimers, we saw a strong increase of chiral optical activity in the plasmonic part (350−900 nm) of the spectrum (Figure 2A,B). This is quite surprising because, to a first approximation, the NP dimers can be represented as a pair of two spheres that has a plane of symmetry, and therefore achiral. Moreover, the chiral anisotropy factor, g, of the heterodimers, 2.05×10^{-2}, is one of the highest obtained so far for any molecular system, although it is smaller than that for a chiroplasmonic layer made on ZnO nanorods, with an out-of-plane alignment with $|g|$ as high as 0.3.[49]

We initially attributed the strong optical activity of the heterodimers to chirality of the constituent NPs.[50] Besides the potentially complex chiral geometries of individual NPs, the mobility of electrons in metals can create a "plasmonic imprint" on metallic NPs from molecules with strong dipoles.[35] However, none of the previously studied cases[35,40,51,52] seem to explain the origin of chiral signals in NP pairs. The starting NPs, without attached CAg or mAb, did not show chiral optical activity at all. The NPs conjugated to CAg or mAb exhibited strong CD signals in the UV region (200−300 nm) corresponding to that of the peptide with $g = 4.6 \times 10^{-3}$. However, the conjugated NPs showed only some chiral optical activity in the visible region (Figure S4). This chiroplasmonic activity is consistent with previous experimental[40,46] and theoretical[52,53] studies but still a lot weaker than the CD signals from dimers, indicating a different origin of optical activity in the heterodimers.

On the basis of the earlier studies,[24,46] we also considered the possibility of concurrent assembly of four different spherical particles along with the dimers due to nonspecific adsorption. Such constructs could be nonplanar and display chirality similar in origin to that of organic molecules. This hypothesis was not proven to be valid here because (1) the amount of multiparticle

dx.doi.org/10.1021/ja4095445 | J. Am. Chem. Soc. 2013, 135, 18629−18636

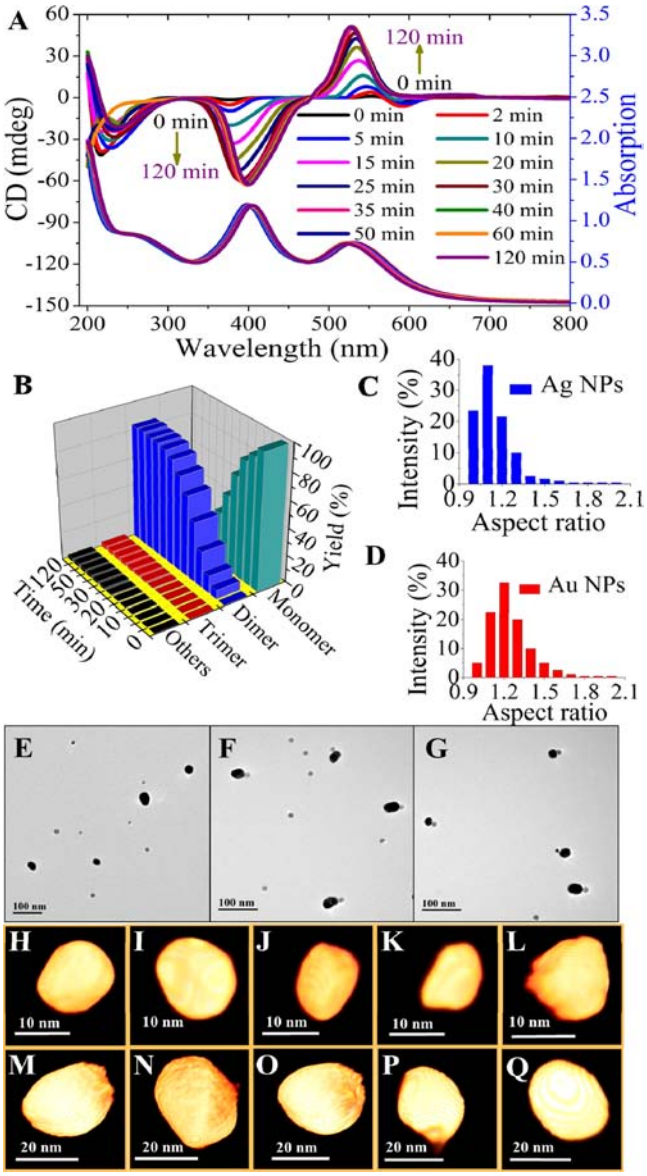

Figure 2. Assembly of heterodimers using mAbs for MCLR. (A) The CD and UV−vis absorption spectra NP heterodimers bridged by mAb-CAg complex acquired at different assembly times. (B) Statistical analysis of the NPs assemblies, counting the number of monomers, dimers, trimers, and others. (C,D) The aspect ratios of NPs determined by bright-field TEM for AgNPs (13 nm) (C) and AuNPs (28 nm) (D). (E−G) Representative TEM images of heterodimers for 0, 20, and 40 min of assembly time, respectively. (H−Q) Representative 3D TEM tomography images of non-assembled AgNPs (H−L) and AuNPs (M−Q).

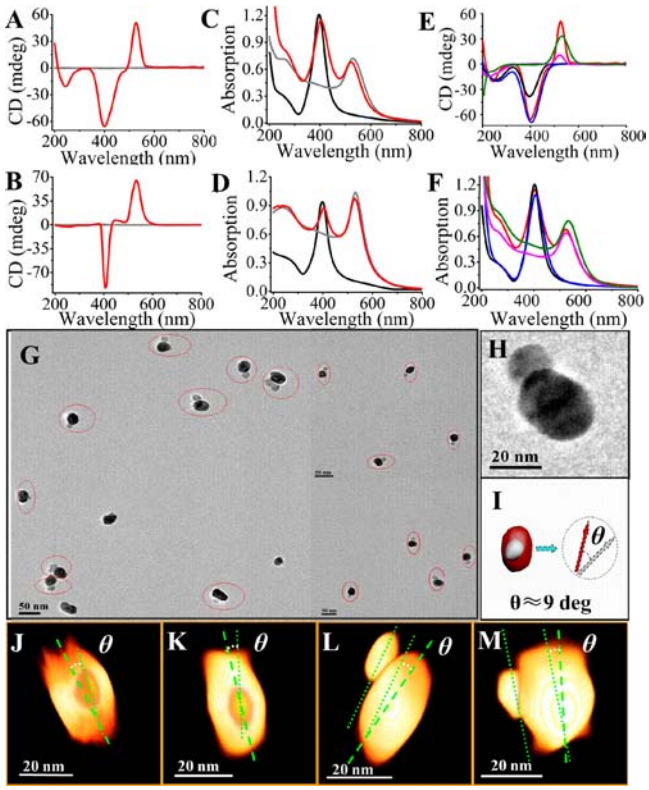

Figure 3. Chiroptical characteristics and geometries for NP heterodimers and homodimers bridged by mAb-CAg immunocomplex specific to MCLR. Experimental (A,C) and theoretical (B,D) CD (A,B) and UV−vis absorption (C,D) spectra for assembled heterodimers (13 nm AgNPs and 28 nm AuNPs, red line) and non-assembled, naked, NPs (13 nm AgNPs, black line; 28 nm AuNPs, gray line). (E,F) CD (E) and UV−vis absorption (F) spectra for AgNP−AuNP heterodimers (13 nm AgNPs and 28 nm AuNPs, red line), AgNP homodimers (13 nm, black line), AgNP homodimers (20 nm, blue line), AuNP homodimers (13 nm, pink line), and AuNP homodimers (28 nm, green line). (G) Representative TEM images of the assembled heterodimers. (H) Zoomed-in TEM image of a heterodimer. (I) Scissor-like geometry of the NP heterodimer, with a dihedral angle between the long axes of NPs marked. (J−M) TEM tomography images of assembled heterodimers. The two constituent prolate NPs are not parallel to each other but have a dihedral angle, θ, between the long NP axes marked with solid and dotted lines.

agglomerates (multimers) containing more than two NPs was less than 3% and (2) their concentration remained unchanged during the same period (20−120 min) of assembly of heterodimers (see Figure 2A,B). Therefore, the chiral activity must be attributed to heterodimers themselves. All the tested permutations of modified and unmodified AgNPs, as well as modified and unmodified AuNPs that could exhibit some nonspecific aggregation, did not lead to the formation of dimers. Likewise, this set of NP permutations showed no or only weak CD bands at 350−900 nm (Figures 3A, 4D, and S4).

In order to address the origin of the heterodimers' chirality, we need to investigate their geometry in much greater detail than was done in the previous studies related to adsorption of proteins on NPs[54,55] and those related to other plasmonic pairs from nanorods.[22] Extensive studies of bright-field TEM images showed that as-made AgNPs and AuNPs deviate substantially from the geometry of a nearly ideal sphere (Figures 2E−G, 3G,H, and S3,S5−S7). Despite the established opinion of these NPs as nearly perfect spheres that dominated previous theoretical and experimental studies, they were found to be prolate ellipsoids. Specifically, the aspect ratios of AgNPs and AuNPs were calculated to be 1.1 and 1.2, respectively, on the basis of the statistical analysis of bright-field TEM images (Figure 2C,D). Concurently, cryo-TEM tomography allowed us to clearly reveal their three-dimensional geometry and identify that they deviate from the spherical shape (Figure 2H−Q). The aspect ratios calculated from the TEM tomography images for AgNPs and AuNPs are 1.14 and 1.22, respectively, which match the geometrical parameters seen in the bright-field images.

dx.doi.org/10.1021/ja4095445 | J. Am. Chem. Soc. 2013, 135, 18629−18636

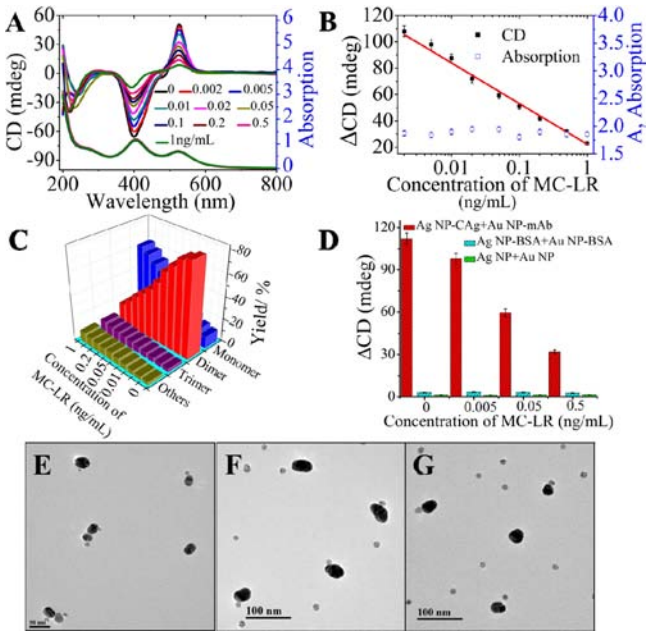

Figure 4. Detection of MCLR by chiroplasmonic technique with NP heterodimers. (A) The CD and UV−vis absorption curves with increasing concentrations of MCLR solution. (B) Calibration curves for MCLR detection, obtained for $\Delta CD = (CD_{526\ nm} - CD_{399\ nm})$ and $A = (A_{523\ nm} + A_{404\ nm})$ as a function of logarithmic MCLR concentrations. (C, D) Comparison of the intensity of the chiroplasmonic signal for heterodimer assemblies from AgNP-CAg and AuNP-mAb with control experiments including (1) a mixture of AgNPs and AuNPs functionalized with BSA and (2) a mixture of AgNPs with AuNPs without mAb or CAg. (E−G) Representative TEM images of assemblies from AgNP-CAg and Au NP-mAb taken after addition of 0.002 (E), 0.1 (F), and 1 ng/mL (G) of MCLR.

TEM tomography also reveals that the two constituent NPs in the heterodimer are not parallel to each other but have a distinct dihedral angle, θ (Figure 3I−M).[22,23,47] The preference for NP dimers with scissor-like conformations, i.e. $\theta \neq 0$, could be explained as the balancing of electrostatic repulsion and attraction forces, as observed for many other nanoscale assemblies with biopolymers.[56] Similarly to the case of spontaneously assembled twisted nanorod pairs,[22,23] the dimers with $\theta > 0$ correspond to the right-handed enantiomer, while the dimers with $\theta < 0$ correspond to the left-handed enantiomer.[22,47] The preference for one enantiomer over the other in the case of the elongated NPs should be attributed to the chirality of the mAb-CAg bridges between them. The presence of plasmonic NPs essentially amplifies this chirality, although not via enhancement of local electrical field or electronic imprint but by acquiring angled conformation with a particularly strong coupling to circularly polarized light.[22,23]

When a photon approaches our scissor-like dimer, two distinct dipoles oriented along the long axis of each NP arise and oscillate in a nonparallel pattern. This contributes to nonzero dipole moment change between the symmetrical and antisymmetric hybrid modes, resulting in a CD signal[57] with a characteristic bisignated line shape.[58] It is important to point out that in this case we refer to the transient dipole moments induced in the NPs by external electromagnetic field rather than permanent dipoles that often determine the geometry of NP assemblies in the ground state.[59,60]

To further understand the origin of chirality, we carried out a computer simulation of the chiroptical properties in the heterodimers using frequency domain finite integral (FDFI) method (Figure 3B), setting the gap between the NPs to be 7 nm according to the DLS results (see Supporting Information and Figure S1). The CD curves of the heterodimers were calculated with various dihedral angles θ from ±2° to ±20°, with a step of 1.5°, considering θ as a variable in the simulations. The heterodimers with θ = +9° gave the best fit between simulated and experimental CD spectra in the 350−600 nm region (Figure 3). The simulated CD spectra showed two strong bands at 406 and 532 nm (Figure 3B); they can be correlated with the 390−410 and 520−530 nm bands observed experimentally (Figure 3A). The theoretical geometry closely coincided with that observed in TEM tomography images (Figure 3J−M).

To confirm the mechanism of chirality for NP dimers, we also investigated optical activity for a variety of other dimers possible in this system (Figure 3E,F). One can notice that the chiroptical activity increases for dimers made from NPs of larger sizes. Taking NPs of the same size, the CD activity is stronger for AgNPs than for AuNPs. Comparison of the chiroptical properties between heterodimers and homodimers shows that the heterodimers possess an advantage of two strong plasmonic CD bands. With a biosensing application in mind, the greater amplitude between the positive and negative peaks of the CD signal and the chiral amplification from plasmonic particles[61,62] may help to achieve better signal-to-noise ratio (SNR) and lower LODs. Hence, the heterodimers were our choice for further studies of their applications in biosensing.

Small Peptide Detection Using Competitive Recognition. We applied chiroplasmonic detection to one of the most pervasive environmental toxins, MCLR. This relatively compact cyclic peptide causes chronic liver damage even for intermittent exposure in small doses; its concentrations in drinking water must be less than 1 ng/mL. When MCLR is present, it competes with CAg on AgNPs to form the NP dimers. Indeed, we found that as the concentration of MCLR increases in solution, the concentration of NP monomers also increases; meanwhile, the concentration of dimers drops (Figures 4C,E−G and S6).

Calibration curves were obtained with respect to the amplitude of the bisignate CD "wave", i.e. from 526 to 399 nm, and displayed excellent linearity over a wide range of concentrations from 0.002 to 0.5 ng/mL. The LOD was determined to be 0.0008 ng/mL (8×10^{-13} M) (Figure 4A,B), which is approximately 1 order of magnitude lower than that of our previous study based on gold nanorod assemblies and other recently reported methods[20,63] for MCLR detection. Importantly, this value is approximately 10 times lower than that of any biosensing method reported so far for all small peptides (Table S1). The LOD for MCLR obtained by ELISA is 0.2 ng/mL (see Supporting Information), which is approximately 250 times higher than that for the chiroplasmonic method. In addition to low LOD, simplicity and speed of the chiroplasmonic method compared with ELISA protocols should also be noted.

It is instructive to compare the chiroplasmonic method with other analytical techniques utilizing plasmonic properties of NPs. As shown in Figure 4B, UV−vis absorption, a commonly used read-out in red−blue plasmon-based colorimetric detection, was not able to detect MCLR. Slight wavelength shifts (2 nm blue shift of silver plasmon band; 1 nm red shift of gold plasmon band) were observed after addition of as much as

dx.doi.org/10.1021/ja4095445 | J. Am. Chem. Soc. 2013, 135, 18629−18636

1 ng/mL of MCLR into the heterodimers solution. Overall, both of the plasmon resonance peaks remained almost unchanged in amplitude and showed no correlation with respect to different concentrations of MCLR. The reason for that, we believe, is a relatively large gap between the particles which prevents strong polaronic coupling and, therefore, the color change. Rotation of the polarization of photons by chiral plasmonic nanoscale assemblies does not necessarily need the direct coupling of excited plasmons.[23] It is primarily based on the independent excitation of plasmons that alters the propagation pattern of the electromagnetic field, and therefore the CD spectrum becomes much more sensitive to the formation of dimers and other plasmonic assemblies when separated by a relatively large gap than methods based on local field enhancement ("hot spots"), exemplified by colorimetry[64] and SERS.[65] The same remains true for surface-enhanced Raman optical activity (SEROA)[66] and field-enhanced CD.[40]

To be comprehensive and provide an adequate comparison with other optical techniques that typically use NP assemblies made from the same metal, we also explored chiroplasmonic and colorimetric detection using CAg-mAb-bridged dimers made only from gold NPs. These were size-asymmetric assemblies composed of a 13 nm AuNP and a 28 nm AuNP (Figure S7). The corresponding detection range and LODs following the chiroplasmonic protocol for detection for MCLR in solution were calculated to be 0.02−1 and 0.01 ng/mL, respectively. Consistent with the results obtained for heterodimers assemblies, colorimetric detection using UV−vis spectra had insufficient sensitivity for this range of concentrations (Figure S7C).

Although the origin of chiral geometry and CD activity is the same for NP hetero- and homodimers, the former are preferred as a bioanalytical tool. The sensitivity of peptide detection was improved by more than 1 order of magnitude for heterodimers in comparison to homodimers. Besides some contribution from enhanced electromagnetic coupling in heterodimers,[31] the difference is attributed to two factors: (1) higher plasmon intensity and therefore stronger polarization rotation for silver NPs when included in the assemblies with gold NPs and (2) the appearance of both positive and negative CD bands, which greatly improved the overall signal and signal-to-noise ratio. The simultaneous presence of two distinct plasmon peaks also contributes to better reliability of bioanalysis using the heterodimers.

In order to understand better the specificity of the developed chiroplasmonic method as an analytical tool for quantitative peptide detection and test for potential alteration of mAb recognition after conjugation to NPs, ochratoxin A (OTA) and another small peptide, glutathione (GSH), were tested as negative controls using the same biosensing protocol with heterodimer assembly as for MCLR (see Figure S8). These experiments showed no cross-reactivity for the target.

Besides confirming the sensitivity and specificity, we also evaluated the practical application of the developed method for water samples from potentially polluted areas that also represent a complex biological mixture. Thus water samples from Tai Lake (JiangSu, China) were spiked with MCLR (Table S2). The results demonstrated excellent recoveries of analyte. The uncertainty factor calculated for these samples was $u(A) = 0.0136$, which is indicative of high reliability of the technique.

Protein Detection by Sandwich Immunoassay Mode. In addition to small peptides such as MCLR, the chiroplasmonic method can be extended to detection of proteins which are larger in size and are more difficult to detect using developed plasmonic techniques due to a greater gap between plasmonic particles and the related exponential decrease of polaron coupling, producing a change in color and/or electric field enhancement. The rotation of polarization is less sensitive to distance between the plasmonic species and therefore can be particularly useful for protein assays.[23]

For this part of the study, we used the so-called "sandwich immunoassay" format. Unlike the competitive recognition assay used for MCLR, in this format the CD signal is expected to increase as the concentration of analyte increases. PSA was chosen as the target analyte for this study because of its (1) clinical significance, (2) molecular weight and other chemical properties typical of cancer biomarkers, and (3) convenience as an analytical model that allows us to make comparisons to other bioanalytical techniques.

AuNPs were modified with the mAb to PSA, while AgNPs were modified with complementary secondary antibody to that PSA mAb, which will be denoted here as smAb. As the concentration of PSA increased, so did the yield of the heterodimers assembled from the functionalized AgNPs and AuNPs (Figures 5 and S10), resulting in the increase of the CD signal, as expected. As a negative control, no CD signal was observed when PSA was added to the system containing only AuNP-mAb (Figure S9) without AgNP-smAb conjugates. Also, no CD signal was observed when PSA was replaced by BSA, indicating specificity of validation in comparison with

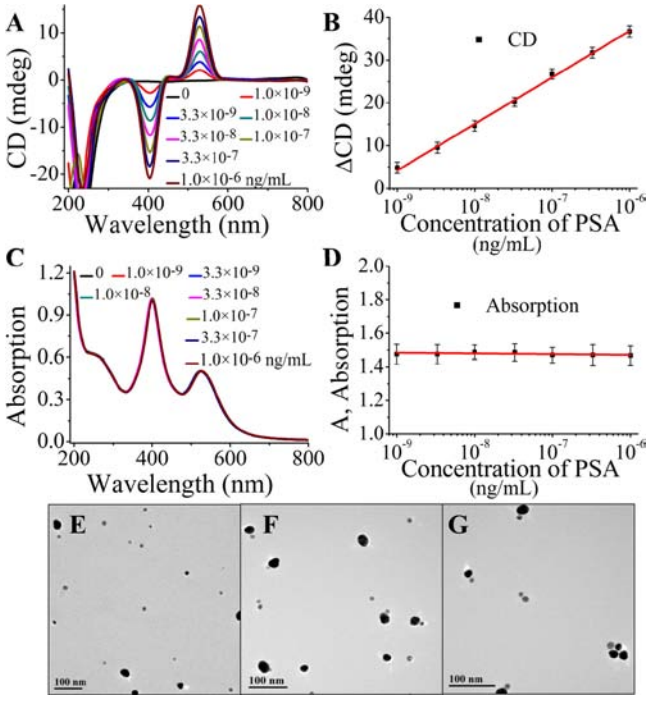

Figure 5. Detection of PSA by chiroplasmonic technique with NP heterodimers. (A,C) The CD (A) and UV−vis absorption (C) curves with increasing concentrations of PSA solution. (B,D) The CD (B) and UV−vis absorption (D) calibration curves for PSA detection, obtained for $\Delta CD = (CD_{530\ nm} - CD_{403\ nm})$ and $A = (A_{527\ nm} + A_{397\ nm})$ as a function of logarithmic PSA concentrations. (E−G) Representative TEM images of heterodimers for PSA detection, taken after addition of 0 (E), 1.0×10^{-8} (F), and 1.0×10^{-6} ng/mL (G) of PSA.

dx.doi.org/10.1021/ja4095445 | J. Am. Chem. Soc. 2013, 135, 18629−18636

albumin—the most abundant protein in the blood (Figure S11).

The *g*-factors of the chiral heterodimers displayed values up to 5×10^{-3} (Figure S12), with the maximum *g*-factor being 8.0 $\times 10^{-3}$. This value is comparable to some of the highest *g*-factors reported for other chiral nanostructures assembled with small molecules,[67,68] DNA,[30,69] peptide/proteins,[34,35] and lipids.[70] As expected the *g*-factors of the heterodimer systems increase with increasing concentration of PSA (Figure S12B).

The detection range and LOD for PSA detection with NP heterodimers were calculated to be 1×10^{-9}–1×10^{-6} and 5×10^{-10} ng/mL (1.5×10^{-20} M), respectively. This LOD is approximately 2 times lower than those of the most sensitive methods available so far, recently reported by Stevens and co-workers.[6,13]

In comparison with the NP-based scanometric immunoassay,[14,71] plasmon resonance shift assay,[5] and other techniques,[6,13,21] the chiroplasmonic assay displays better sensitivity, which should be attributed to the same reasons as those we delineated for the case of MCLR.

Besides the analysis of PSA in phosphate buffer, we also examined the possibility of PSA detection in a complex biological matrix, such as serum. Importantly, we found that chiroplasmonic analysis is robust and selective enough to withstand interferences from multiple peptides and proteins present in serum, which is promising for clinical applications (Table S3).

CONCLUSION

In summary, AgNP–AuNP dimers were assembled with high yield by using antibody–antigen bridges. The unexpected chirality and CD bands appearing in the visible region of the absorption spectrum was attributed to the nonspherical shape of the NPs that can be better described as prolate ellipsoids with aspect ratio of 1.1-1.2. Their dimers acquire scissor-like conformation with long axes of the NPs forming a dihedral angle of about 9 degrees. Plasmonic enhancement of the chirality of the biomolecular bridges between the NPs, the bisignate nature of the CD bands, and an unusual dependence of the intensity of CD bands on the distance between the NPs enabled exceptionally low LODs for both small and peptides/proteins. More than one order of magnitude improvement for bioanalysis of environmental toxin MCLR and a cancer marker PSA were obtained. Such sensitivity was retained in complex media with multiple biological components. Also, the chiroplasmonic method of bioanalysis is quicker and simpler than the plasmonic ELISA assay[13] and reveals better LODs than other NP-based techniques.[5,71] Note, however, chiroplasmonic detection will need more complex optical instrumentation than red-blue colorimetric assays assays utilizing Au NPs.

EXPERIMENTAL SECTION

Assembly of NP Dimers. First, 1000 μL portions of AuNP (28 ± 3.1 nm) and AgNP (13 ± 1.8 nm) colloids were adjusted to pH 8.5 with 0.1 M Na_2CO_3 before being conjugated with anti-MCLR mAb (9.5 μL, 100 μg/mL) and CAg (the conjugation of MCLR to BSA) (14 μL, 50 μg/mL), respectively, under gentle stirring.[5,48] Thereafter, the solutions were incubated for 1 h at room temperature and blocked by BSA (13.5 μL, 500 μg/mL) for 30 min. Next, the functionalized gold and silver solutions were centrifuged for 10 min at 6000 and 13000 rpm, respectively. After the supernatants were discarded, the precipitates were redispersed in 1000 μL of 10 mM phosphate buffer (PB) solutions and finally mixed together for the assembly of AgNP–AuNP heterodimers. The reaction was completed within 40 min, which is common for the formation of antigen–antibody immunocomplexes. Note that for the detection of the biomacromolecule PSA, a classic sandwich immunoassay format was used instead of the competition protocol above, in which PSA was captured by AuNP-mAb and AgNP-smAb, while for the assembly of AuNP dimers, the procedures were exactly the same except for replacement of AgNP colloids with AuNPs (13 ± 2.1 nm).

Pollutants Detection. A stock solution of MCLR (10 μg/mL) was prepared in 10 mM PB solution. From this, the MCLR solution was consecutively diluted to 100, 50, 20, 10, 5, 2, 1, 0.5, 0.2, and 0 ng/mL as the working solutions. Then, 20 μL samples of each solution were added to a different prepared NP dimer solution. After incubation, CD was collected for each sample. To probe the viability of this method for implementation in real samples with no need for any complicated pretreatment protocol, the experiment was carried out using water from Tai Lake (Wuxi, China) spiked with MCLR[72] and studied by CD spectra as previously described (see Table S2).

Clinical Biomarker Detection. PSA sera, sampled from healthy male donors at the Second Hospital in Wuxi, were confirmed by the standard clinical diagnostic assay (ADVIA Centaur, Siemens). Additional serial dilution (in bovine serum) was needed before detection with the developed method, as the concentrations of PSA in sera were outside the scale of the analysis methods used here. The experiment was approved by the Ethics Committee of the Second Hospital.

Computer Simulations of Optical Properties. The frequency domain finite integral method was used to calculate the chiroptical properties of the homodimers and heterodimers. The calculations are detailed in the Supporting Information.

ASSOCIATED CONTENT

Supporting Information

Additional experimental details; supplementary figures and tables.This material is available free of charge via the Internet at http://pubs.acs.org.

AUTHOR INFORMATION

Corresponding Authors

kuangh@jiangnan.edu.cn
kotov@umich.edu

Author Contributions

#X.W. and L.X. contributed equally.

Notes

The authors declare no competing financial interest.

ACKNOWLEDGMENTS

This work is financially supported by the National Natural Science Foundation of China (21071066, 91027038, 21101079, 21175034, 21371081, 21301073), the Key Programs from MOST (2012BAC01B07, 2012BAD29B04, 2012BAK17B10, 2012BAK08B01, 2012YQ090194), and grants from Jiangsu Province, MOF and MOE (NCET-12-0879, BE2011626, JUSRP51308A). This study was partially supported by the Center for Solar and Thermal Energy Conversion, an Energy Frontier Research Center under the auspices of the U.S. Department of Energy, Office of Science, Office of Basic Energy Sciences under Award No. DE-SC0000957. We acknowledge support from NSF under grant ECS-0601345; EFRI-BSBA 0938019; CBET 0933384; CBET 0932823; and CBET 1036672. The work is also partially supported by ARO MURI W911NF-12-1-0407 "Coherent Effects in Hybrid Nanostructures for Lineshape Engineering of Electromagnetic Media" (N.A.K.).

REFERENCES

(1) Saha, K.; Agasti, S. S.; Kim, C.; Li, X.; Rotello, V. M. *Chem. Rev.* **2012**, *112*, 2739.
(2) Choi, Y.; Park, Y.; Kang, T.; Lee, L. P. *Nat. Nanotechnol.* **2009**, *4*, 742.
(3) Anker, J. N.; Hall, W. P.; Lyandres, O.; Shah, N. C.; Zhao, J.; Van Duyne, R. P. *Nat. Mater.* **2008**, *7*, 442.
(4) Sönnichsen, C.; Reinhard, B. M.; Liphardt, J.; Alivisatos, A. P. *Nat. Biotechnol.* **2005**, *23*, 741.
(5) Hall, W. P.; Ngatia, S. N.; Van Duyne, R. P. *J. Phys. Chem. C* **2011**, *115*, 1410.
(6) Rodríguez-Lorenzo, L.; de La Rica, R.; Álvarez-Puebla, R. A.; Liz-Marzán, L. M.; Stevens, M. M. *Nat. Mater.* **2012**, *11*, 604.
(7) Mohs, A. M.; Mancini, M. C.; Singhal, S.; Provenzale, J. M.; Leyland-Jones, B.; Wang, M. D.; Nie, S. *Anal. Chem.* **2010**, *82*, 9058.
(8) Cho, H.; Baker, B. R.; Wachsmann-Hogiu, S.; Pagba, C. V.; Laurence, T. A.; Lane, S. M.; Lee, L. P.; Tok, J. B. H. *Nano Lett.* **2008**, *8*, 4386.
(9) Rodríguez-Lorenzo, L.; Alvarez-Puebla, R. A.; Pastoriza-Santos, I.; Mazzucco, S.; Stéphan, O.; Kociak, M.; Liz-Marzán, L. M.; García de Abajo, F. J. *J. Am. Chem. Soc.* **2009**, *131*, 4616.
(10) Liu, X.; Wang, F.; Niazov-Elkan, A.; Guo, W.; Willner, I. *Nano Lett.* **2013**, *13*, 309.
(11) Freeman, R.; Girsh, J.; Fang-ju Jou, A.; Ho, J.-a. A.; Hug, T.; Dernedde, J.; Willner, I. *Anal. Chem.* **2012**, *84*, 6192.
(12) Xie, P.; Xiong, Q.; Fang, Y.; Qing, Q.; Lieber, C. M. *Nat. Nanotechnol.* **2012**, *7*, 119.
(13) de la Rica, R.; Stevens, M. M. *Nat. Nanotechnol.* **2012**, *7*, 821.
(14) Nam, J.-M.; Thaxton, C. S.; Mirkin, C. A. *Science* **2003**, *301*, 1884.
(15) Thaxton, C. S.; Elghanian, R.; Thomas, A. D.; Stoeva, S. I.; Lee, J. S.; Smith, N. D.; Schaeffer, A. J.; Klocker, H.; Horninger, W.; Bartsch, G.; Mirkin, C. A. *Proc. Natl. Acad. Sci. U.S.A.* **2009**, *106*, 18437.
(16) Punj, D.; Mivelle, M.; Moparthi, S. B.; van Zanten, T. S.; Rigneault, H.; van Hulst, N. F.; Garcia-Parajo, M. F.; Wenger, J. *Nat. Nanotechnol.* **2013**, *8*, 512.
(17) Lim, D.-K.; Jeon, K.-S.; Kim, H. M.; Nam, J.-M.; Suh, Y. D. *Nat. Mater.* **2010**, *9*, 60.
(18) Xia, F.; Zuo, X.; Yang, R.; Xiao, Y.; Kang, D.; Vallée-Bélisle, A.; Gong, X.; Yuen, J. D.; Hsu, B. B. Y.; Heeger, A. J. *Proc. Natl. Acad. Sci. U.S.A.* **2010**, *107*, 10837.
(19) Turner, A. P. F. *Chem. Soc. Rev.* **2013**, *42*, 3184.
(20) Wang, L.; Zhu, Y.; Xu, L.; Chen, W.; Kuang, H.; Liu, L.; Agarwal, A.; Xu, C.; Kotov, N. A. *Angew. Chem., Int. Ed.* **2010**, *49*, 5472.
(21) Hendry, E.; Carpy, T.; Johnston, J.; Popland, M.; Mikhaylovskiy, R.; Lapthorn, A.; Kelly, S.; Barron, L.; Gadegaard, N.; Kadodwala, M. *Nat. Nanotechnol.* **2010**, *5*, 783.
(22) Ma, W.; Kuang, H.; Wang, L.; Xu, L.; Chang, W.-S.; Zhang, H.; Sun, M.; Zhu, Y.; Zhao, Y.; Liu, L.; Xu, C.; Link, S.; Kotov, N. A. *Sci. Rep.* **2013**, *3*, 1934.
(23) Ma, W.; Kuang, H.; Xu, L.; Ding, L.; Xu, C.; Wang, L.; Kotov, N. A. *Nat. Commun.* **2013**, *4*, 2689.
(24) Chen, W.; Bian, A.; Agarwal, A.; Liu, L.; Shen, H.; Wang, L.; Xu, C.; Kotov, N. A. *Nano Lett.* **2009**, *9*, 2153.
(25) Kuzyk, A.; Schreiber, R.; Fan, Z.; Pardatscher, G.; Roller, E.-M.; Högele, A.; Simmel, F. C.; Govorov, A. O.; Liedl, T. *Nature* **2012**, *483*, 311.
(26) Mastroianni, A. J.; Claridge, S. A.; Alivisatos, A. P. *J. Am. Chem. Soc.* **2009**, *131*, 8455.
(27) Shen, X.; Asenjo-Garcia, A.; Liu, Q.; Jiang, Q.; García de Abajo, F. J.; Liu, N.; Ding, B. *Nano Lett.* **2013**, *13*, 2128.
(28) Shen, X.; Song, C.; Wang, J.; Shi, D.; Wang, Z.; Liu, N.; Ding, B. *J. Am. Chem. Soc.* **2012**, *134*, 146.
(29) Shemer, G.; Krichevski, O.; Markovich, G.; Molotsky, T.; Lubitz, I.; Kotlyar, A. B. *J. Am. Chem. Soc.* **2006**, *128*, 11006.
(30) Zhao, Y.; Xu, L.; Liz-Marzán, L. M.; Kuang, H.; Ma, W.; Asenjo-García, A.; García de Abajo, F. J.; Kotov, N. A.; Wang, L.; Xu, C. *J. Phys. Chem. Lett.* **2013**, *4*, 641.
(31) Zhang, H.; Govorov, A. O. *Phys. Rev. B* **2013**, *87*, 075410.
(32) Song, C.; Blaber, M. G.; Zhao, G.; Zhang, P.; Fry, H. C.; Schatz, G. C.; Rosi, N. L. *Nano Lett.* **2013**, *13*, 3256.
(33) Chen, C.-L.; Zhang, P.; Rosi, N. L. *J. Am. Chem. Soc.* **2008**, *130*, 13555.
(34) George, J.; Thomas, K. G. *J. Am. Chem. Soc.* **2010**, *132*, 2502.
(35) Slocik, J. M.; Govorov, A. O.; Naik, R. R. *Nano Lett.* **2011**, *11*, 701.
(36) Hendler, N.; Fadeev, L.; Mentovich, E. D.; Belgorodsky, B.; Gozin, M.; Richter, S. *Chem. Commun.* **2011**, *47*, 7419.
(37) Kobayashi, M.; Tomita, S.; Sawada, K.; Shiba, K.; Yanagi, H.; Yamashita, I.; Uraoka, Y. *Opt. Exp.* **2012**, *20*, 24856.
(38) Oh, H. S.; Liu, S.; Jee, H. S.; Baev, A.; Swihart, M. T.; Prasad, P. N. *J. Am. Chem. Soc.* **2010**, *132*, 17346.
(39) Wang, S.; Mamedova, N.; Kotov, N. A.; Chen, W.; Studer, J. *Nano Lett.* **2002**, *2*, 817.
(40) Lieberman, I.; Shemer, G.; Fried, T.; Kosower, E. M.; Markovich, G. *Angew. Chem., Int. Ed.* **2008**, *47*, 4855.
(41) (a) Shukla, N.; Bartel, M. A.; Gellman, A. J. *J. Am. Chem. Soc.* **2010**, *132*, 8575. (b) Torres, T.; Bottari, G.; Amabilino, D. B., *Chiral Organic Nanomaterials*; John Wiley & Sons, Inc.: New York, 2013.
(42) Smith, D. R.; Pendry, J. B.; Wiltshire, M. C. K. *Science* **2004**, *305*, 788.
(43) Plum, E.; Zhou, J.; Dong, J.; Fedotov, V. A.; Koschny, T.; Soukoulis, C. M.; Zheludev, N. I. *Phys. Rev. B* **2009**, *79*, 035407.
(44) Corma, A.; Serna, P. *Science* **2006**, *313*, 332.
(45) Zhu, Y.; Qian, H.; Drake, B. A.; Jin, R. *Angew. Chem., Int. Ed.* **2010**, *49*, 1295.
(46) Yan, W.; Xu, L.; Xu, C.; Ma, W.; Kuang, H.; Wang, L.; Kotov, N. A. *J. Am. Chem. Soc.* **2012**, *134*, 15114.
(47) Auguié, B.; Alonso-Gómez, J. L.; Guerrero-Martínez, A. s.; Liz-Marzán, L. M. *J. Phys. Chem. Lett.* **2011**, *2*, 846.
(48) Tung, N. H.; Chikae, M.; Ukita, Y.; Viet, P. H.; Takamura, Y. *Anal. Chem.* **2012**, *84*, 1210.
(49) Yeom, B.; Zhang, H.; Zhang, H.; Park, J. I.; Kim, K.; Govorov, A. O.; Kotov, N. A. *Nano Lett.* **2013**, *13*, 5277.
(50) Fan, Z.; Govorov, A. O. *Nano Lett.* **2012**, *12*, 3283.
(51) Zhou, Y.; Yang, M.; Sun, K.; Tang, Z.; Kotov, N. A. *J. Am. Chem. Soc.* **2010**, *132*, 6006.
(52) Govorov, A. O. *J. Phys. Chem. C* **2011**, *115*, 7914.
(53) Berova, N.; Nakanishi, K.; Woody, R. W. *Circular dichroism: principles and applications*; Wiley-VCH: New York, 2000; Vol. 2.
(54) Tsai, D.-H.; DelRio, F. W.; Keene, A. M.; Tyner, K. M.; MacCuspie, R. I.; Cho, T. J.; Zachariah, M. R.; Hackley, V. A. *Langmuir* **2011**, *27*, 2464.
(55) Walczyk, D.; Bombelli, F. B.; Monopoli, M. P.; Lynch, I.; Dawson, K. A. *J. Am. Chem. Soc.* **2010**, *132*, 5761.
(56) Gibaud, T.; Barry, E.; Zakhary, M. J.; Henglin, M.; Ward, A.; Yang, Y.; Berciu, C.; Oldenbourg, R.; Hagan, M. F.; Nicastro, D.; Meyer, R. B.; Dogic, Z. *Nature* **2012**, *481*, 348.
(57) Prodan, E.; Radloff, C.; Halas, N. J.; Nordlander, P. *Science* **2003**, *302*, 419.
(58) Guerrero-Martínez, A.; Alonso-Gómez, J. L.; Auguié, B.; Cid, M. M.; Liz-Marzán, L. M. *Nano Today* **2011**, *6*, 381.
(59) Shanbhag, S.; Kotov, N. A. *J. Phys. Chem. B* **2006**, *110*, 12211.
(60) Tang, Z.; Kotov, N. A.; Giersig, M. *Science* **2002**, *297*, 237.
(61) García de Abaj, F. J. *J. Phys. Chem. C* **2008**, *112*, 17983.
(62) Zhao, J.; Pinchuk, A. O.; McMahon, J. M.; Li, S.; Ausman, L. K.; Atkinson, A. L.; Schatz, G. C. *Acc. Chem. Res.* **2008**, *41*, 1710.
(63) Ng, A.; Chinnappan, R.; Eissa, S.; Liu, H.; Tlili, C.; Zourob, M. *Environ. Sci. Technol.* **2012**, *46*, 10697.
(64) Guo, L.; Xu, Y.; Ferhan, A. R.; Chen, G.; Kim, D.-H. *J. Am. Chem. Soc.* **2013**, *135*, 12338.
(65) Qian, X.; Li, J.; Nie, S. *J. Am. Chem. Soc.* **2009**, *131*, 7540.
(66) Abdali, S.; Blanch, E. W. *Chem. Soc. Rev.* **2008**, *37*, 980.

(67) Dolamic, I.; Knoppe, S.; Dass, A.; Bürgi, T. *Nat. Commun.* **2012**, *3*, 798.
(68) Gautier, C.; Bürgi, T. *J. Am. Chem. Soc.* **2006**, *128*, 11079.
(69) Molotsky, T.; Tamarin, T.; Moshe, A. B.; Markovich, G.; Kotlyar, A. B. *J. Phys. Chem. C* **2010**, *114*, 15951.
(70) Wang, R.-Y.; Wang, H.; Wu, X.; Ji, Y.; Wang, P.; Qu, Y.; Chung, T.-S. *Soft Matter* **2011**, *7*, 8370.
(71) Kim, D.; Daniel, W. L.; Mirkin, C. A. *Anal. Chem.* **2009**, *81*, 9183.
(72) Wang, L.; Chen, W.; Xu, D.; Shim, B. S.; Zhu, Y.; Sun, F.; Liu, L.; Peng, C.; Jin, Z.; Xu, C. *Nano Lett.* **2009**, *9*, 4147.